Monthly Notices
of the
ROYAL ASTRONOMICAL SOCIETY

MNRAS **452,** 1754–1763 (2015) doi:10.1093/mnras/stv1395

The first pre-supersoft X-ray binary

S. G. Parsons,[1⋆] M. R. Schreiber,[1,2] B. T. Gänsicke,[3] A. Rebassa-Mansergas,[4] R. Brahm,[5,6] M. Zorotovic,[1] O. Toloza,[3] A. F. Pala,[3] C. Tappert,[1] A. Bayo[1,2] and A. Jordán[5,6]

[1]*Instituto de Física y Astronomía, Universidad de Valparaíso, Avenida Gran Bretana 1111, Valparaíso 2360102, Chile*
[2]*Millenium Nucleus 'Protoplanetary Disks in ALMA Early Science', Universidad de Valparaiso, Valparaiso 2360102, Chile*
[3]*Department of Physics, University of Warwick, Coventry CV4 7AL, UK*
[4]*Kavli Institute for Astronomy and Astrophysics, Peking University, Beijing 100871, China*
[5]*Instituto de Astrofsica, Facultad de Fsica, Pontificia Universidad Católica de Chile, Av. Vicuña Mackenna 4860, 7820436 Macul, Santiago, Chile*
[6]*Millennium Institute of Astrophysics, Av. Vicuña Mackenna 4860, 7820436 Macul, Santiago, Chile*

Accepted 2015 June 22. Received 2015 June 15; in original form 2015 March 25

ABSTRACT

We report the discovery of an extremely close white dwarf plus F dwarf main-sequence star in a 12 h binary identified by combining data from the Radial Velocity Experiment survey and the *Galaxy Evolution Explorer* survey. A combination of spectral energy distribution fitting and optical and *Hubble Space Telescope* ultraviolet spectroscopy allowed us to place fairly precise constraints on the physical parameters of the binary. The system, TYC 6760-497-1, consists of a hot $T_{\rm eff} \sim 20\,000$ K, $M_{\rm WD} \sim 0.6\,{\rm M}_{\odot}$ white dwarf and an F8 star ($M_{\rm MS} \sim 1.23\,{\rm M}_{\odot}$, $R_{\rm MS} \sim 1.3\,{\rm R}_{\odot}$) seen at a low inclination ($i \sim 37^{\circ}$). The system is likely the descendant of a binary that contained the F star and an $\sim$2 $\rm M_{\odot}$ A-type star that filled its Roche lobe on the thermally pulsating asymptotic giant branch, initiating a common envelope phase. The F star is extremely close to Roche lobe filling and there is likely to be a short phase of thermal time-scale mass transfer on to the white dwarf during which stable hydrogen burning occurs. During this phase, it will grow in mass by up to 20 per cent, until the mass ratio reaches close to unity, at which point it will appear as a standard cataclysmic variable star. Therefore, TYC 6760-497-1 is the first known progenitor of a supersoft source system, but will not undergo a Type Ia supernova explosion. Once an accurate distance to the system is determined by *Gaia*, we will be able to place very tight constraints on the stellar and binary parameters.

Key words: binaries: close – stars: early-type – stars: evolution – white dwarfs.

1 INTRODUCTION

The unique properties of Type Ia supernovae (SN Ia) as distance indicators, sufficiently bright to serve as yardsticks on cosmological scales (e.g. Branch & Tammann 1992), has resulted in them becoming some of the most important objects in the Universe, having led to the discovery of its accelerating expansion (Riess et al. 1998; Perlmutter et al. 1999).

Although it is generally accepted that SN Ia are related to the thermonuclear ignition of a white dwarf that surpassed the Chandrasekhar mass limit, there is no consensus yet on the pathways leading to the explosion. The two main formation channels are thought to be the 'single-degenerate' channel, where a white dwarf accretes material from a non-degenerate companion via Roche lobe overflow (Whelan & Iben 1973) during a phase of thermal time-scale mass transfer known also as the supersoft source (SSS) phase, and the 'double-degenerate' channel in which the explosion is the result of the merger of two white dwarfs (Webbink 1984). In recent years, the idea of a 'double-detonation' scenario has also been advanced. In this case, a layer of helium on the surface of the white dwarf detonates, triggering the explosion of the underlying core either directly or via a compressional shock wave (Fink, Hillebrandt & Röpke 2007; Fink et al. 2010; Shen & Moore 2014); hence, it is possible via this channel to detonate the white dwarf while its mass is still below the Chandrasekhar limit. In theory, these 'sub-Chandrasekhar SN Ia' are possible via both main channels. In the single-degenerate channel, the white dwarf accretes helium-rich material from a donor star, building up a large surface layer (Tutukov & Yungelson 1996), whilst the merger of a carbon–oxygen core white dwarf with a low-mass helium core white dwarf can lead to helium ignition and hence a supernova via the double-degenerate channel (Fink et al. 2007).

The search for Galactic SN Ia progenitors from either of the channels is a difficult task. In the single-degenerate case, very few SSS systems sufficiently nearby for detailed parameter

⋆ E-mail: steven.parsons@uv.cl

studies are known (Greiner 2000). This is due to a combination of the short duration of the SSS phase and because their very soft X-ray emission is easily absorbed by neutral hydrogen in the galactic plane. Whilst double white dwarf binaries are intrinsically faint objects and difficult to distinguish from single white dwarfs without dedicated spectroscopic monitoring (see Napiwotzki et al. 2003, for example). However, in both cases the progenitor systems are the descendants of detached white dwarf plus F-, G- or early K-type main-sequence star companions. With no ongoing accretion, these systems are easy to characterize. Furthermore, they are expected to be numerous (Holberg et al. 2013) and so are optimal for population studies and hence testing both SN Ia progenitor channels.

However, identifying white dwarfs with early-type companions has been extremely difficult until recently. This is due to the fact that the main-sequence star completely outshines the white dwarf at optical wavelengths (Rebassa-Mansergas et al. 2012a); hence, a combination of optical and ultraviolet (UV) coverage is required to find these systems. Maxted et al. (2009) attempted to detect systems of this type by combining data from the *Galaxy Evolution Explorer* (*GALEX*) survey and the Sloan Digital Sky Survey, but were limited by the optical colour selection of their main-sequence stars, whilst Burleigh, Barstow & Fleming (1997) found only four unresolved white dwarf plus FGK main-sequence star systems searching for extreme-UV and soft X-ray excesses.

We have recently begun a project combining the large data set of the RAdial Velocity Experiment (RAVE) survey (Kordopatis et al. 2013) in the Southern hemisphere and the LAMOST (Large Sky Area Multi-Object Fiber Spectroscopic Telescope) survey in the Northern hemisphere, with UV data from the *GALEX* survey in order to identify main-sequence F, G and early K stars with significant UV excesses.

The RAVE survey spectroscopically observed more than 400 000 bright ($8 < I < 12$ mag) Southern hemisphere stars in the spectral region 8410–8794 Å (the infrared calcium triplet) with a resolution of $R \sim 7000$. The data were used to establish the basic parameters of each star (effective temperatures, surface gravities and metallicities) as well as line-of-sight velocities. We used these data, in conjunction with PHOENIX synthetic spectra (Husser et al. 2013), to estimate the UV colours of these stars. We selected those showing UV-excess flux for radial velocity follow-up observations to detect close binarity, as well as *Hubble Space Telescope* (*HST*) UV spectroscopy to confirm the presence of a white dwarf. Full details of this process and the list of UV-excess objects will be published in a forthcoming paper (Parsons et al., in preparation).

As well as providing a crucial test of the single-degenerate channel for SN Ia, these detached white dwarf plus early-type main-sequence star binaries also provide useful constraints for the common envelope phase of binary evolution, which they passed through when the progenitor of the white dwarf evolved off the main sequence. Essentially, all current observational constraints on the common envelope phase are based on systems containing white dwarfs with low-mass M dwarf companions (e.g. Zorotovic et al. 2010). However, the handful of systems with more massive main-sequence star components already hint that additional energy may be needed to expel the envelope in these cases (Zorotovic, Schreiber & Parsons 2014).

In this paper, we present data for the first of our UV-excess objects from the RAVE sample to be confirmed as a close white dwarf plus main-sequence binary. The object, TYC 6760-497-1, is a late-F star. We derive clear observational constraints on the stellar and binary parameters of the systems, reconstruct its evolutionary history, predict its future and discuss the implications for our understanding of close compact binary star evolution.

2 OBSERVATIONS AND THEIR REDUCTION

2.1 Optical echelle spectroscopy

2.1.1 FEROS and the du Pont echelle

We obtained high-resolution spectroscopy of TYC 6760-497-1 with the echelle spectrograph ($R \sim 40\,000$) on the 2.5 m du Pont telescope located at Las Campanas Observatory, Chile and with FEROS ($R \sim 48\,000$) on the 2.2 m Telescope at La Silla, Chile. FEROS covers the wavelength range from ∼3500 to ∼9200 Å. The observations formed part of a programme to detect binarity among a large number of potential white dwarf plus main-sequence binaries. However, it was immediately clear that TYC 6760-497-1 had a very short period when we observed a very large velocity shift between our first two measurements. Therefore, we obtained several spectra of this target per night throughout the rest of the observing run with the aim of measuring its period.

Data obtained with the FEROS and du Pont spectrographs were extracted and analysed with an automated pipeline developed to process spectra coming from different instruments in an homogeneous and robust manner (Jordán et al. 2014; Brahm et al., in preparation). After performing typical image reductions, spectra were optimally extracted following Marsh (1989) and calibrated in wavelength using reference ThAr Lamps. For FEROS data, the instrumental drift in wavelength through the night was corrected with a secondary fibre observing a ThAr lamp. In the case of the du Pont data, ThAr spectra were acquired before and after each science observation. Wavelength solutions were shifted to the barycentre of the Solar system.

2.1.2 X-shooter

A medium-resolution spectrum ($R \sim 5000$) of TYC 6760-497-1 was obtained with X-shooter (D'Odorico et al. 2006) mounted at the Cassegrain focus of VLT-UT2 at Paranal on 2015 February 26. X-shooter is comprised of three detectors that enable one to obtain simultaneous data from the UV cutoff at 0.3 μm to the *K* band at 2.4 μm. Our data consisted of three 60 s exposures, which were reduced using the standard pipeline release of the X-shooter Common Pipeline Library recipes (version 2.5.2). The instrumental response was removed and the spectrum flux was calibrated by observing the spectrophotometric standard star CD-38 10980 and dividing it by a flux table of the same star to produce the response function. The spectrum was extinction corrected but not corrected for telluric features.

2.2 UV spectroscopy

TYC 6760-497-1 was observed with the *HST* on 2015 January 9 with the Space Telescope Imaging Spectrograph (STIS) as part of programme GO 13704. We used the G140L grating centred on 1425 Å, for one spacecraft orbit, resulting in a total exposure time of 2381 s. The data were processed using CALSTIS V3.4. We dereddened the STIS spectrum using a value of $E(B - V) = 0.103$, determined from our spectral energy distribution (SED) fit to the main-sequence star (see Section 4.1).

Table 1. Radial velocity measurements for the main-sequence star in TYC 6760-497-1.

BJD (mid-exposure)	Velocity ($km\,s^{-1}$)	Uncertainty ($km\,s^{-1}$)	Telescope/ instrument
2456811.5672390	30.33	0.50	du Pont/Echelle
2456827.6293689	−48.79	0.48	MPG2.2/FEROS
2456828.4841811	53.36	0.28	MPG2.2/FEROS
2456828.5729529	−13.12	0.28	MPG2.2/FEROS
2456828.5904822	−26.22	0.28	MPG2.2/FEROS
2456828.6012976	−34.38	0.27	MPG2.2/FEROS
2456828.6663049	−61.48	0.30	MPG2.2/FEROS
2456828.6775301	−63.33	0.30	MPG2.2/FEROS
2456828.7213267	−55.85	0.28	MPG2.2/FEROS
2456829.5163187	32.99	0.29	MPG2.2/FEROS
2456829.5491571	7.39	0.27	MPG2.2/FEROS
2456829.5939247	−29.35	0.30	MPG2.2/FEROS
2456829.6737526	−62.99	0.31	MPG2.2/FEROS
2456829.6855582	−61.90	0.29	MPG2.2/FEROS
2456829.6963120	−60.80	0.29	MPG2.2/FEROS
2456829.7123239	−58.27	0.29	MPG2.2/FEROS
2456829.7603942	−33.58	0.30	MPG2.2/FEROS
2456829.7718605	−24.86	0.29	MPG2.2/FEROS
2456829.7818813	−15.99	0.28	MPG2.2/FEROS
2456834.6122883	−49.91	0.30	MPG2.2/FEROS
2456834.6226973	−52.15	0.29	MPG2.2/FEROS
2456835.7338779	−41.03	0.29	MPG2.2/FEROS

3 RESULTS

3.1 Optical spectra

Radial velocities were computed from our optical echelle spectra using the cross-correlation technique against a binary mask representative of a G2-type star. The uncertainties in radial velocity were computed using scaling relations (for more details, see Jordán et al. 2014) with the signal-to-noise ratio and width of the cross-correlation peak, which were calibrated with Monte Carlo simulations. The results are listed in Table 1. We note, however, that these relations were calibrated using slowly rotating stars and hence the uncertainties may be underestimated for rapidly rotating stars, such as the one in TYC 6760-497-1.

We also estimated the projected rotational velocity ($v_{\rm rot}\sin i$) of the main-sequence star in TYC 6760-497-1 by comparing the observed FEROS spectra against a synthetic grid of stellar spectra (Coelho et al. 2005). The synthetic spectra were degraded to the resolution of FEROS by convolving them with a Gaussian with $R = \lambda/\delta\lambda = 53\,000$ and then further degraded to different values of $v_{\rm rot}\sin i$ using the limb-darkening coefficients of Claret (2004). The optimal fit (which also yields a set of stellar parameters) was found by chi-square minimization in 3 echelle order of the spectra which include the zone of the magnesium triplet (5000–5500 Å). The measured rotational broadening was $v_{\rm rot}\sin i = 75 \pm 3\ {\rm km\,s^{-1}}$. We also obtained the following stellar parameters: $T_{\rm eff} = 5750 \pm 200$ K, $\log g = 3.75 \pm 0.3$ (in cgs units), [Fe/H] $= -0.5 \pm 0.2$. Fig. 1 shows the observed spectra with the best-fitting model, as well as the same model with no rotational broadening. This high rotation rate means that the fitted stellar parameters from the spectral fit are not necessarily reliable since most of the weak lines that have a $\log g$ dependence are completely smeared out. Moreover, the system is extremely close to Roche lobe filling (see Section 4) and hence the effects of gravity darkening and Roche distortion likely have an effect on the spectral fit.

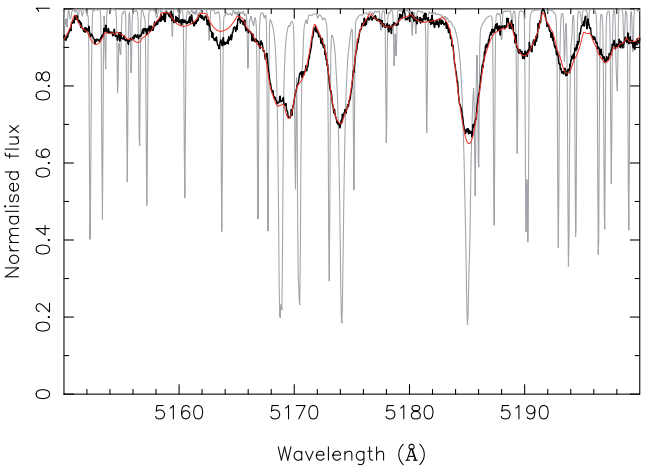

Figure 1. Observed FEROS spectrum (black line) of TYC 6760-497-1 with the best-fitting model overplotted (red line, $v_{\rm rot}\sin i = 75\,{\rm km\,s^{-1}}$). We also plot the model spectra without any rotational broadening (grey line) to highlight the rapid rotation of the star.

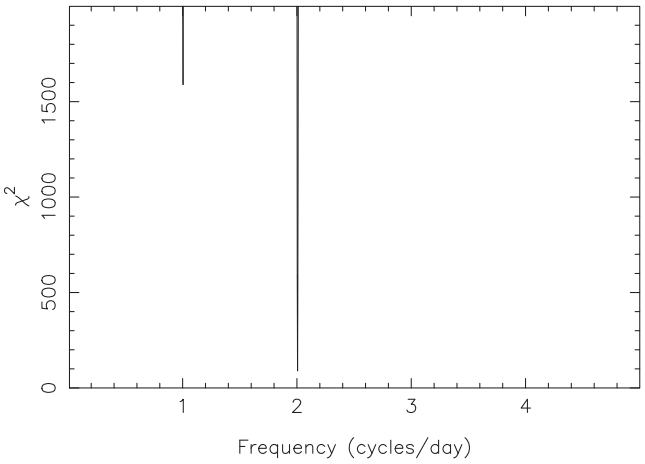

Figure 2. χ^2 plotted against orbital period for the fit to the radial velocity measurements. There is a clear minimum at a period of 0.5 d.

3.2 Orbital period

We measured the binary period of TYC 6760-497-1 by fitting a constant plus sine wave to the velocity measurements over a range of periods and computing the χ^2 of the resulting fit. The result of this is shown in Fig. 2 and shows a clear minimum in χ^2 at a period of 0.5 d. We determine the ephemeris of TYC 6760-497-1 as

$$\mathrm{BJD} = 2456823.81993(40) + 0.498688(26)E, \quad (1)$$

where E is the binary phase and phase 0 occurs at the conjunction of the main-sequence star.

The phase-folded radial velocity plot is shown in Fig. 3. We find a radial velocity semi-amplitude for the main-sequence star of $65.0 \pm 0.3\,{\rm km\,s^{-1}}$ and a systemic velocity of $1.4 \pm 0.2\,{\rm km\,s^{-1}}$. The lower panel of Fig. 3 shows the residuals to the fit, which show variations larger than their uncertainties. This is likely due to the main-sequence star's large rotational broadening causing small systematic errors during the cross-correlation process.

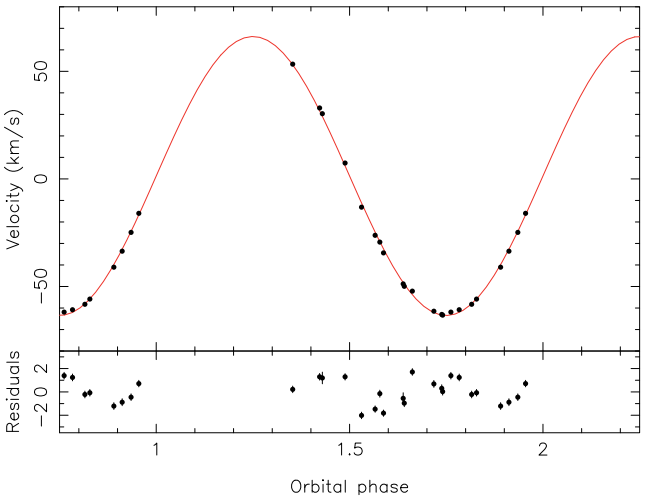

Figure 3. Phase-folded radial velocity plot for the main-sequence star in TYC 6760-497-1. The lower panel shows the residuals to the best fit.

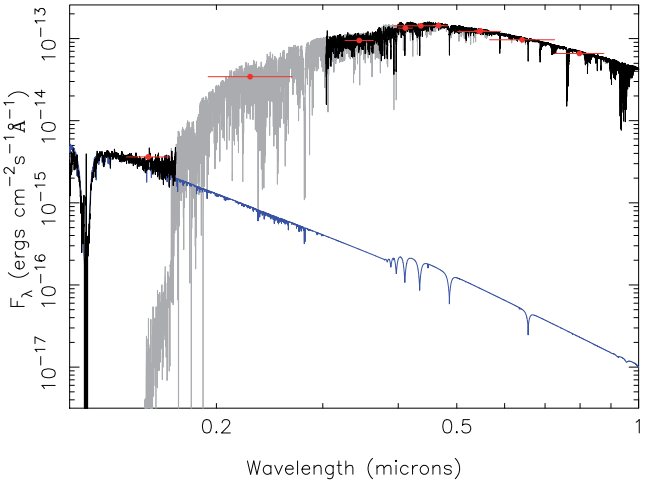

Figure 4. The SED of TYC 6760-497-1 in the UV and optical wavelength ranges (the SED fit also included infrared data, but we limit the plot to this range to demonstrate the relative contributions of the two stars). The black lines are the observed UV *HST*/STIS spectrum and optical X-shooter spectrum (no telluric correction was applied). Broad-band photometry is shown in red (their errors are too small to see on this scale); the best-fitting BTSettl main-sequence star model is shown in grey and was rotationally broadened to match the measured value for the main-sequence star in TYC 6760-497-1. We also plot in dark blue a TLUSTY/SYNSPEC model for a $T_{\rm eff} = 20\,400$ K, $\log g = 8$ white dwarf. The fit to the UV part of the spectrum is better illustrated in Fig. 7.

4 SYSTEM PARAMETERS

In this section, we detail how we constrained the physical parameters of the binary.

4.1 SED fit

In order to get an initial estimate of the physical parameters of the main-sequence star in TYC 6760-497-1 and the reddening towards the system, we fitted its SED using the virtual observatory SED analyzer (VOSA; Bayo et al. 2008). We convolved our flux-calibrated X-shooter spectrum with a number of generic narrow- and broad-band filters including Strömgren *uvby*, Bessell *BVRI* Johnson *BVR* and Cousins *RI* filters. We combined these with archival data from the *GALEX* (Martin et al. 2005), 2MASS (Skrutskie et al. 2006) and *WISE* (Wright et al. 2010) catalogues. We excluded the *GALEX* data when fitting the SED since we expected the white dwarf to contribute a non-negligible amount of flux at these wavelengths.

We used a large grid of BTSettl (Allard, Homeier & Freytag 2012) models to determine the main-sequence star's parameters and allowed the extinction to vary from zero to three times the maximum expected value of $A_{\rm V} = 0.36$ (Schlafly & Finkbeiner 2011). As expected, the fit was insensitive to the metallicity of the system and only mildly sensitive to the surface gravity, preferring a value of $\log g \sim 4.0$. However, we found that the temperature was well constrained to $T_{\rm eff} = 6400 \pm 100$ K and the extinction to be $A_{\rm V} = 0.32$, implying $E(B-V) = 0.103$, in good agreement with what is expected from the Schlafly & Finkbeiner (2011) maps. The uncertainties were determined via a Bayes analysis (for more details, see Bayo et al. 2008). These measurements are consistent with those from the RAVE survey, in which TYC 6760-497-1 was determined to have $T_{\rm eff} = 6150 \pm 100$ K and $\log g = 3.6 \pm 0.2$ (Kordopatis et al. 2013), although these measurements are likely affected by the large rotational broadening, similar to our FEROS fit. In Fig. 4, we show part of the SED in the UV and optical wavelength ranges with the best-fitting model and observed spectra overplotted. While the *GALEX* NUV measurement shows little evidence of an excess, the FUV measurement is clearly dominated by the white dwarf.

4.2 Rotational broadening constraint

Assuming that the main-sequence star is tidally locked to the white dwarf, which it should be since the tidal synchronisation time-scale for this system is less than 0.5 Myr (Zahn 1977), much shorter than the white dwarf's cooling age (see Section 5.1), the rotational broadening measurement can be used to place some constraints on the binary parameters via

$$v_{\rm rot} \sin i = K_{\rm MS}(1+q)\frac{R_{\rm MS}}{a}, \quad (2)$$

where $K_{\rm MS}$ is the radial velocity semi-amplitude of the main-sequence star, $q = M_{\rm MS}/M_{\rm WD}$, the mass ratio of the binary and $R_{\rm MS}/a$ is the radius of the main-sequence star scaled by the orbital separation. Combining this with Kepler's third law,

$$a^3 = \frac{P^2 G M_{\rm MS}}{4\pi^2}\left(1+\frac{1}{q}\right), \quad (3)$$

where P is the orbital period and G is the gravitational constant, we can effectively solve for q (hence $M_{\rm WD}$) by assuming a mass and radius for the main-sequence star. Once this is known, all the other binary parameters can then be determined. For example, the orbital inclination via

$$\sin^3 i = \frac{P K_{\rm MS}^2 (1+q)^2}{2\pi G M_{\rm WD}}. \quad (4)$$

Ideally, the fit to the FEROS spectra would yield the main-sequence star's effective temperature, surface gravity and metallicity, which can then be used to estimate its mass and radius via the Torres relation (Torres, Andersen & Giménez 2010) and hence determine the binary parameters. Unfortunately, due to its rapid rotation, the FEROS fit does not give reliable stellar parameters. Therefore, keeping the metallicity fixed at the solar value, we used a grid of $T_{\rm eff}$, $\log g$ values and the Torres relation to determine the range of possible binary parameters. The result of this is shown in Fig. 5. We

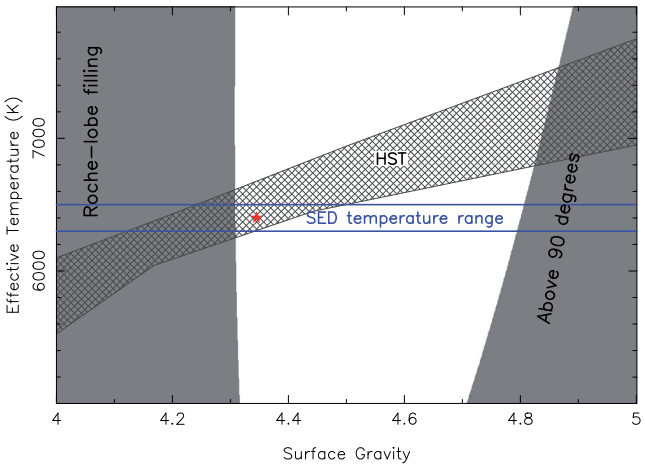

Figure 5. Limits on the physical parameters of the main-sequence star. The measured rotational broadening, period and radial velocity amplitude exclude the light grey areas as at low surface gravities the star fills its Roche lobe, whilst high surface gravities lead to unphysical results. The horizonal blue lines indicate the possible temperature range from the SED fit. The dark grey hatched area indicates the parameter range that is consistent with the fit to the white dwarf's spectrum (see Section 4.3). The small region that is consistent with all our constraints is highlighted by a red star symbol.

found that at surface gravities below ∼4.3, the binary parameters were such that the main-sequence star should be Roche lobe filling. Since there is no evidence for this, we can exclude this region. Furthermore, at very high surface gravities (>4.8), a solution to the binary parameters is not possible since it would require the inclination to be larger than 90 deg. Hence, this region can also be excluded. However, this still results in a large range of possible parameters; the white dwarf mass can be anything between 0.3 and 0.7 $M_{\odot}$, the main-sequence star mass between 1.08 and 1.26 $M_{\odot}$ and the inclination larger than 32 deg. Varying the metallicity does not have a large effect on these limits.

We estimated the distance to TYC 6760-497-1 using isochrones from the Padova and Trieste Stellar Evolution Code (Bressan et al. 2012). For a given temperature, we used the isochrones to calculate the absolute magnitude of the main-sequence star over the full range of allowed surface gravities in the *BVRIJHK* bands and compared these to the measured values to calculate the distance. This results in a range of distances for a given main-sequence star temperature. We take into account the variations in the calculated distances from the different bands and the effects of the unknown age of the star. The result of this is shown in Fig. 6. While the unknown age of the star generally has little effect on the predicted distance, if it is very young (<30 Myr, which is in fact ruled out by the cooling age of the white dwarf) or very old (>3.2 Gyr), the resultant distance is somewhat larger than whilst on the main-sequence.

4.3 White dwarf spectral fit

We fitted the *HST*/STIS spectrum of the white dwarf in TYC 6760-497-1 with a grid of white dwarf models computed using TLUSTY/SYNSPEC (Hubeny & Lanz 1995), stepping in surface gravity from 7.0 to 9.5 in steps of 0.1 (see Fig. 7). At each step, the best fit to the spectrum gives the temperature and hence the mass and radius using the cooling models of Fontaine, Brassard & Bergeron (2001). Scaling the flux then also gives an estimate of the distance. Hence, we are able to determine the white dwarf mass, effective temperature and distance as a function of the surface gravity. These

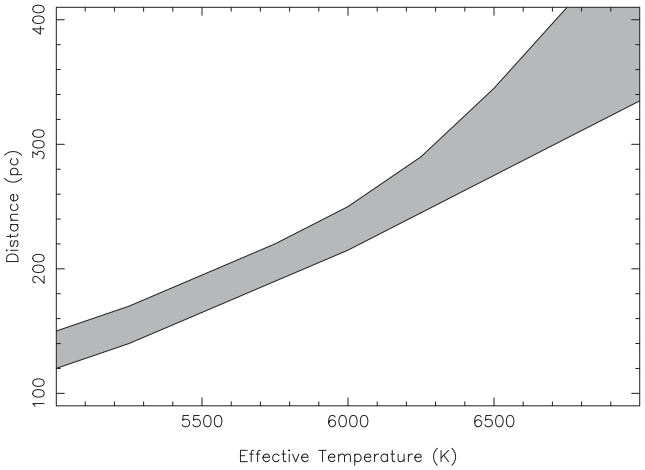

Figure 6. Distance to the main-sequence star in TYC 6760-497-1 as a function of its effective temperature. The grey region shows the permitted range.

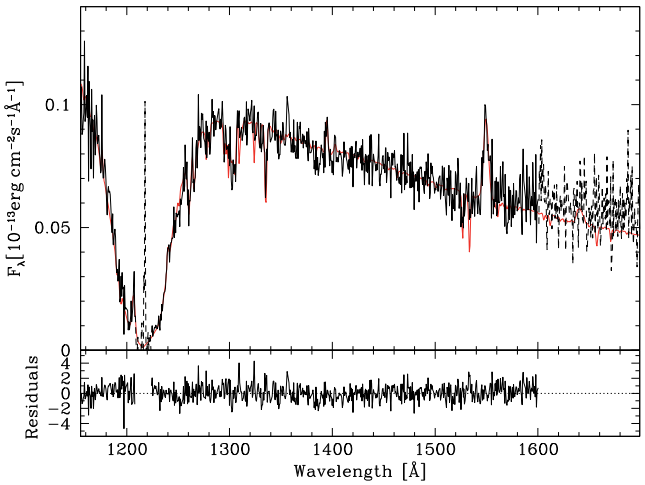

Figure 7. *HST*/STIS spectrum of the white dwarf in TYC 6760-497-1 with a model fit overplotted (red line, $\log g = 8.0$). The dashed parts were not included in the fit; these include the core of the Lyα line, which is contaminated by geocoronal emission, and the red end of the spectrum, which has low signal-to-noise. There are also several emission lines including the quite strong C IV 1550 Å line. These are likely due to the white dwarf capturing material from the wind of the F star.

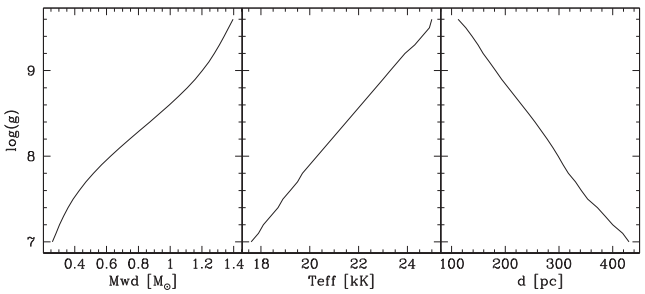

Figure 8. Constraints on the white dwarf's parameters as a function of its surface gravity.

relations are illustrated in Fig. 8. $T_{\rm eff}$ and $\log g$ are correlated parameters, so increasing $\log g$ results in a higher best-fitting $T_{\rm eff}$. At the same time, increasing $\log g$ implies a higher mass, and, via the mass–radius relation, a smaller radius. This drop in radius

dominates over the increase in $T_{\rm eff}$ in the UV flux emitted by the white dwarf, i.e. increasing the surface gravity leads to a lower best-fitting distance.

Several narrow absorption features are seen in the STIS spectrum, primarily from Si and C as a result of the white dwarf accreting material from the wind of the main-sequence star as is commonly seen in other close white dwarf binaries (Tappert et al. 2011; Parsons et al. 2012; Pyrzas et al. 2012; Ribeiro et al. 2013). We found that setting the metal abundances in the model to 0.1 times solar for all elements fits these well.

4.4 Combined constraints

We can combine the constraints from fitting the white dwarf's spectrum with those from the main-sequence star to determine which set of parameters are consistent with all our data. For a given main-sequence star effective temperature, we have a range of possible distances from the isochrone fitting (see Fig. 6), which then leads to a range of possible white dwarf masses from the relations shown in Fig. 8. The rotational broadening measurement also yields a white dwarf mass for a given main-sequence star temperature and gravity, allowing us to determine the range over which these two measurements are consistent. This range is shown in Fig. 5 as the dark grey hatched region. We can instantly exclude a main-sequence star with a temperature less than ∼6200 K, since a star this cool would be at a short distance and hence would have a white dwarf with a mass $>0.7\,{\rm M}_{\odot}$, which is only possible if the system fills its Roche lobe. It also means that the system must be at a minimum distance of 250 pc.

These constraints are also consistent with those from the main-sequence star temperature determined from the SED fitting ($T_{\rm eff} = 6400 \pm 100$ K), which is also illustrated in Fig. 5. There is therefore a small region in which all of our measurements and fits are consistent, highlighted by a red star in Fig. 5. The full set of ranges for all the parameters are given in Table 2.

Table 2. Physical and binary parameters of TYC 6760-497-1.

Parameter	Value
RA	15:02:22.4896
Dec.	−29:41:15.666
B	11.578
V	11.245
R	11.030
J	10.167
H	9.918
K	9.853
Distance (pc)	250–320
Orbital period (d)	0.498 688(26)
$K_{\rm MS}$ ($\rm km\,s^{-1}$)	65.0 ± 0.3
$v_{\rm rot} \sin i$ ($\rm km\,s^{-1}$)	75.0 ± 3.0
Inclination (°)	33–43
Separation ($\rm R_{\odot}$)	3.20–3.28
White dwarf mass ($\rm M_{\odot}$)	0.52–0.67
White dwarf temperature (K)	19 500–21 000
Main-sequence star spectral type	F8
Main-sequence star temperature (K)	6300–6500
Main-sequence star surface gravity	4.31–4.48
Main-sequence star mass ($\rm M_{\odot}$)	1.22–1.25
Main-sequence star radius ($\rm R_{\odot}$)	1.18–1.40

5 DISCUSSION

Having determined the stellar and binary parameters of TYC 6760-497-1, we can now investigate the evolution of the system and its implications for models of compact binary star evolution and SN Ia formation channels. We start by reconstructing the system evolutionary history.

5.1 Constraints on common envelope evolution

Common envelope evolution is typically described with a parametrized energy equation:

$$E_{\rm bind} = \alpha_{\rm CE} \Delta E_{\rm orb}, \tag{5}$$

where $\alpha_{\rm CE}$ represents the fraction of orbital energy that is used to unbind the envelope usually called the common envelope efficiency (Paczynski 1976).

The binding energy of the envelope is often assumed to be equal to the gravitational energy of the envelope:

$$E_{\rm bind} = E_{\rm gr} = -\frac{G M_1 M_{1,\rm e}}{\lambda R_1}, \tag{6}$$

where M_1, $M_{1,\rm e}$ and R_1 are the total mass, envelope mass and radius of the primary star, and λ is a binding energy parameter. Although very often ignored, the binding energy parameter strongly depends on the mass and evolutionary state of the white dwarf progenitor when filling its Roche lobe. This is especially true if the recombination energy $U_{\rm rec}$ available within the envelope supports the ejection process. Therefore, a more general form for the binding energy equation is

$$E_{\rm bind} = \int_{M_{1,\rm c}}^{M_1} -\frac{Gm}{r(m)} {\rm d}m + \alpha_{\rm rec} \int_{M_{1,\rm c}}^{M_1} U_{\rm rec}(m), \tag{7}$$

where $\alpha_{\rm rec}$ is the fraction of recombination energy that contributes to the ejection process. It is of outstanding importance for our understanding of compact binary star evolution to observationally constrain the values of both common envelope efficiencies and to investigate possible dependences on the binary parameters.

With its period of less than half a day, TYC 6760-497-1 is the first short orbital period ($P_{\rm orb} < 1$ d) post-common envelope binary (PCEB) with a massive secondary star (spectral type earlier than K). The two systems that have been previously discovered are IK Peg and KOI-3278 with much longer orbital periods of 21.722 and 88.18 d, respectively (Wonnacott, Kellett & Stickland 1993; Kruse & Agol 2014). These two systems would have formed through common envelope evolution only if the common envelope efficiency $\alpha_{\rm CE}$ has been larger than it seems to be required to understand PCEBs with M dwarf secondaries, where $\alpha_{\rm CE} \sim 0.25$–$0.5$ seems to work best (Zorotovic et al. 2010; Rebassa-Mansergas et al. 2012b; Toonen & Nelemans 2013; Camacho et al. 2014) and/or if in addition to a high fraction of the released orbital energy also recombination energy contributed to some degree to the ejection process expelling the envelope (Zorotovic et al. 2010, 2014).

To investigate whether TYC 6760-497-1 confirms or disproves the trend of larger efficiencies being required to understand PCEBs with massive secondaries, we follow Zorotovic et al. (2010) and reconstruct the evolutionary history of the system using the binary star evolution code BSE (Hurley, Tout & Pols 2002) and the parameter constraints derived in the previous sections, i.e. $M_{\rm WD} = 0.52$–$0.67\,{\rm M}_{\odot}$, $M_{\rm MS} = 1.22$–$1.25\,{\rm M}_{\odot}$, $P_{\rm orb} = 0.498\,688$ d and $T_{\rm eff,\,WD} = 19\,500$–$21\,000$ K. The current cooling age of the white dwarf is only ∼0.1 Gyr (Fontaine et al. 2001); hence, the

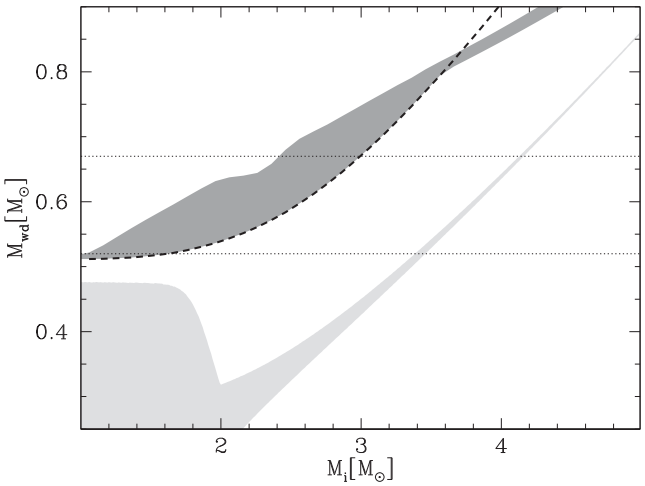

Figure 9. The mass of the white dwarf after the common envelope phase as a function of its initial progenitor mass. The resultant white dwarf mass depends heavily upon the evolutionary stage at which the common envelope started. We show the results for a progenitor on the first giant branch (light grey), on the early AGB (dashed line) and on the TP-AGB (dark grey). The horizontal lines correspond to the range of white dwarf masses in agreement with our observations.

current orbital period is virtually identical to the period the system had at the end of the common envelope (even if efficient magnetic braking is assumed). Reconstructing the common envelope evolution as in Zorotovic et al. (2014), we find a large range of possible values for the common envelope efficiencies for TYC 6760-497-1 and different possible evolutionary stages at which the progenitor of the white dwarf could have filled its Roche lobe.

Fig. 9 shows the solutions with $\alpha_{CE} < 1$ in a final versus initial mass plot for the primary if contributions from recombination energy are ignored (i.e. $\alpha_{rec} = 0.0$). Solutions exist for massive progenitors on the first giant branch (FGB), on the early asymptotic giant branch (AGB) and on the thermally pulsating-AGB (TP-AGB). The more massive the progenitor, the larger the value of the common envelope efficiency must have been and the younger is the system today. The possible ranges are $\alpha = 0.90$–1.0 for a 3.40–4.13 $M_\odot$ progenitor that fills its Roche lobe on the FGB (becoming first a naked helium star then eventually a carbon–oxygen white dwarf; Hurley et al. 2002) at an age of 0.17–0.27 Gyr; $\alpha = 0.08$–0.89 if the progenitor reached the early AGB, after 0.48–2.49 Gyr and with an initial mass of 1.61–2.99 $M_\odot$; and finally $\alpha_{CE} = 0.05$–0.20 for a 1.37–2.99 $M_\odot$ progenitor that filled its Roche lobe on the TP-AGB at an age of 0.48–4.15 Gyr, making it the oldest option. In the latter case, we get the largest ranges as the core mass on the TP-AGB reaches the current white dwarf mass for a large range of initial masses. We therefore consider this the most likely scenario. This is further supported by our measurement of the radius of the secondary. Assuming solar metallicity a 1.235 $M_\odot$ main-sequence star needs ∼1.8 Gyr to expand from its zero-age main sequence (ZAMS) radius to the current radius of the secondary of 1.35 $R_\odot$. We therefore conclude that the most consistent scenario for the evolutionary history of TYC 6760-497-1 is that the progenitor of the white dwarf was of a relatively low mass (∼2 $M_\odot$) and filled its Roche lobe on the TP-AGB, which implies that the common envelope efficiency must have been small $\alpha_{CE} = 0.05$–0.20. This is much smaller than values obtained for the long orbital period systems with secondary stars of similar mass (IK Peg and KOI-3278). In addition, contributions from recombination energy are not required to understand the existence of TYC 6760-497-1. If recombination energy contributed to expelling the envelope of the progenitor of the white dwarf, the fraction of orbital energy lost during the common envelope is reduced even further while the possible initial masses would remain virtually identical. It therefore seems that a simple dependence of the total common envelope efficiency on the secondary mass as speculated by Zorotovic et al. (2014) remains an incomplete prescription for common envelope evolution and other parameters such as perhaps the evolutionary state of the progenitor when it fills its Roche lobe may play an important role. Characterizing more PCEBs with massive secondaries is therefore urgently required to progress with our understanding of compact binary evolution which is directly related to our understanding of SN Ia progenitor systems.

5.2 The future of TYC 6760-497-1

While it is clear that PCEBs with M dwarf secondaries evolve into cataclysmic variables (CVs) as long as the mass transfer will be dynamically stable, the future of PCEBs with more massive secondary stars is more uncertain and potentially very interesting as the total mass of the binary usually exceeds the Chandrasekhar limit. Indeed, PCEBs with massive (G- or F-type) secondaries are the progenitors of SN Ia explosions for both the double- and the single-degenerate channel. If the separation of a given PCEB is large, it potentially survives a second common envelope forming a double-degenerate system which may then merge and produce an SN Ia. If, on the other hand, the system is close, it might start thermal time-scale mass transfer and reach the rates required for stable nuclear burning on the surface of the white dwarf allowing its mass to increase and potentially reach the Chandrasekhar limit.

With its short orbital period and given that the system is rather young, TYC 6760-497-1 will clearly start mass transfer before the secondary evolves off the main sequence. It is also clear that the system will not undergo dynamical time-scale mass transfer as the critical mass ratio for dynamically unstable mass transfer is $q_{cr} \gtrsim 2.5$ (Ge et al. 2013) for donor stars with masses and radii similar to the Sun. It is less clear, however, if the mass transfer will be thermally stable (i.e. stable against thermal time-scale mass transfer). The critical mass ratio for marginal stability against thermal time-scale mass transfer in a semi-detached binary star can be obtained by equating the mass–radius exponent of the Roche lobe and the star, i.e.

$$\zeta_{th} = \frac{d\ln(R_{MS})}{d\ln(M_{MS})} = \frac{d\ln(R_L)}{d\ln(M_{MS})} \quad (8)$$

(see also e.g. de Kool 1992), where the Roche lobe radius (R_L) is a function of the mass ratio and the binary separation. Despite the secondary in TYC 6760-497-1 being slightly evolved, we can get a first hint about the future of the system by calculating the limit implied by equation (8) using the ZAMS M–R relation from Tout et al. (1996). For conservative mass transfer, we get a critical mass ratio for thermal time-scale mass transfer of $q_{cr} = 1.4$–1.48 for TYC 6760-497-1. Thus, in the case of conservative mass transfer, the system will certainly experience thermal time-scale mass transfer.

However, the assumption of conservative mass transfer is not necessarily correct. As long as the mass transfer rate stays below the critical value for stable hydrogen burning on the white dwarf, mass transfer will most likely not be conservative. Instead, nova eruptions will occur, the white dwarf mass will remain nearly constant and angular momentum will be taken away from the system

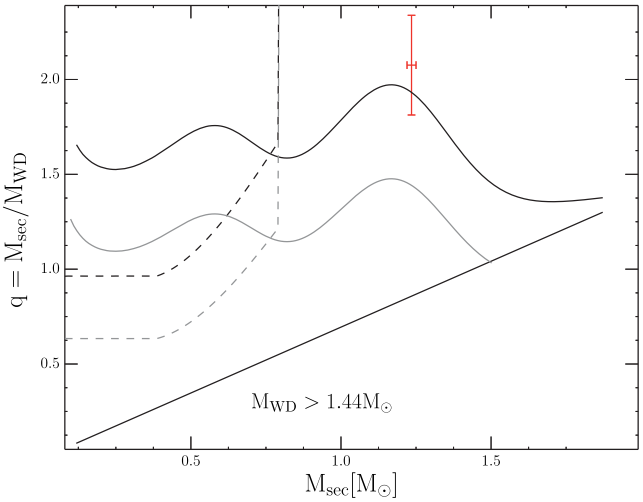

Figure 10. Critical mass ratio for thermal time-scale mass transfer as a function of the main-sequence star's mass for conservative (grey) and non-conservative (black) mass transfer. The position of TYC 6760-497-1 is indicated in red. For completeness, we also provide the limits for dynamical time-scale mass transfer (dashed lines) where we used the fits to detailed calculations of the adiabatic mass–radius exponent (Hjellming 1989).

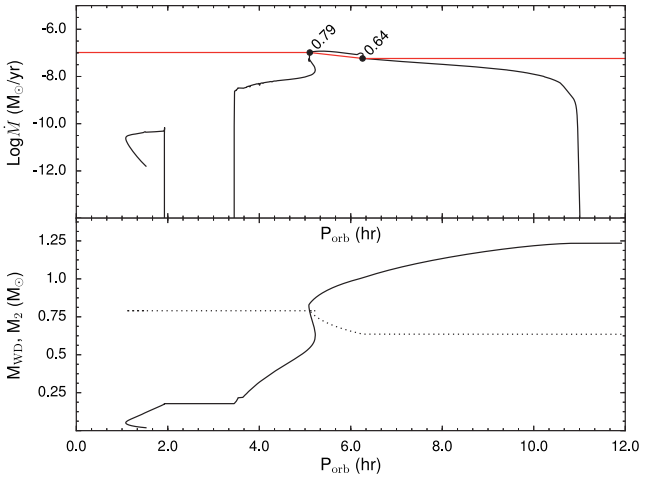

Figure 11. The predicted future evolution of the mass transfer rate (top panel), the white dwarf mass (dotted line, bottom panel) and the secondary star mass (solid line, bottom panel) as a function of orbital period. The horizontal red line in the top panel represents the mass transfer rate required for stable hydrogen burning for the respective mass of the white dwarf (i.e. when the mass transfer rate is above this line, stable hydrogen burning occurs). At $P_{\rm orb} \sim 6.5$ h, TYC 6760-497-1 reaches this critical mass transfer rate. As a consequence, mass transfer becomes conservative and the white dwarf grows in mass. At $P_{\rm orb} \sim 5$ h, the white dwarf mass has reached $0.79\,{\rm M}_\odot$ and the mass transfer rate drops below the rate required for stable burning. At this moment, TYC 6760-497-1 becomes a 'normal' CV with non-conservative stable mass transfer driven by angular momentum loss only and a constant white dwarf mass.

by the expelled material. In Fig. 10, we show the critical values for the mass ratio as a function of secondary mass for both conservative and non-conservative mass transfer. In the latter case, we assume the mass expelled during nova eruptions to carry the specific angular momentum of the white dwarf. The white dwarf mass is assumed to be constant and the mass (and angular momentum) loss to be continuous which has been shown to be equivalent to a discontinuous sequence of nova cycles in terms of the secular evolution of CVs (Schenker, Kolb & Ritter 1998). These assumptions are typical assumptions for CVs (e.g. Ritter 1988). The position of TYC 6760-497-1 is very close to the limit for thermal time-scale mass transfer in the case of non-conservative mass transfer so the system may indeed be a progenitor of an SSS.

In order to investigate the future of TYC 6760-497-1 in more detail, we performed dedicated simulations using MESA (Paxton et al. 2011). We assume the initial masses of the two stars to be $M_{\rm MS} = 1.235\,{\rm M}_\odot$ and $M_{\rm WD} = 0.63\,{\rm M}_\odot$ and secondary radius of $1.35\,{\rm R}_\odot$, which corresponds to the mean values of the ranges in agreement with our observations. The starting model was obtained by evolving the secondary until it reaches the required radius (after 1.8 Gyr) and the white dwarf is approximated as a point mass. We assume mass transfer to be nearly conservative (90 per cent of the transferred mass remains on the white dwarf) if the mass transfer is large enough to generate stable hydrogen burning on the surface of the white dwarf as we run into numerical problems in the fully conservative case. For mass transfer rates below the limit for stable burning, we assume that all the accreted mass is expelled during nova eruptions leaving the system with the specific angular momentum of the white dwarf. Finally, for angular momentum loss due to magnetic braking, we assume the standard prescription from Rappaport, Verbunt & Joss (1983).

Based on these assumptions, the future of TYC 6760-497-1 can be estimated. The black line in the top panel of Fig. 11 shows the predicted mass transfer rate of TYC 6760-497-1 as a function of orbital period. At an orbital period of 11.9 h (in less than 5 Myr), mass transfer will start. The mass transfer rate will quickly increase as the system is thermally unstable, but does not reach the limit for stable hydrogen burning until the system has an orbital period of 6.2 h (13.1 Myr from now). At this point, mass transfer becomes conservative (we assume that 90 per cent of the burned material remains on the white dwarf). As a consequence, the mass transfer rate increases significantly and the white dwarf mass grows (bottom panel). When the white dwarf mass reaches $0.79\,{\rm M}_\odot$ (14.1 Myr from now), the mass ratio will be close to unity (secondary mass of $0.8\,{\rm M}_\odot$ at an orbital period of 5.1 h) and the system becomes stable against (conservative) thermal time-scale mass transfer. Therefore, the accretion rate drops below the value required for stable hydrogen burning. From this moment on, TYC 6760-497-1 will behave as expected for normal CVs: after 105 Myr it will enter the period gap and restart mass transfer at a much lower rate at an orbital period of 2.1 h (1.5 Gyr from now). Finally, the system will reach the orbital period minimum (∼1.1 h) 4.8 Gyr from now.

While the predicted final evolution of the period and mass transfer rate of TYC 6760-497-1 is identical to those of CVs descending from PCEBs with less massive secondaries, its past as a PCEB containing a more massive secondary star will be imprinted in the relative abundances of carbon and nitrogen of the accreted material as soon as the outer convection zone reaches regions containing CNO processed material. Decreased values for C/N and C_{12}/C_{13} in CVs descending from thermal time-scale mass transfer systems have been predicted by Schenker et al. (2002) and found in CVs based on the presence of C/N line ratios measured with *HST* by Gänsicke et al. (2003). In Fig. 12, we predict the C/N and C_{12}/C_{13} abundance ratios for TYC 6760-497-1 as a function of orbital period. As soon as the secondary star starts to develop a deep convective envelope, both surface abundance ratios decrease significantly. Most dramatically, C/N decreases by several orders of magnitude. TYC 6760-497-1 is therefore likely a progenitor of the CVs with decreased C/N line

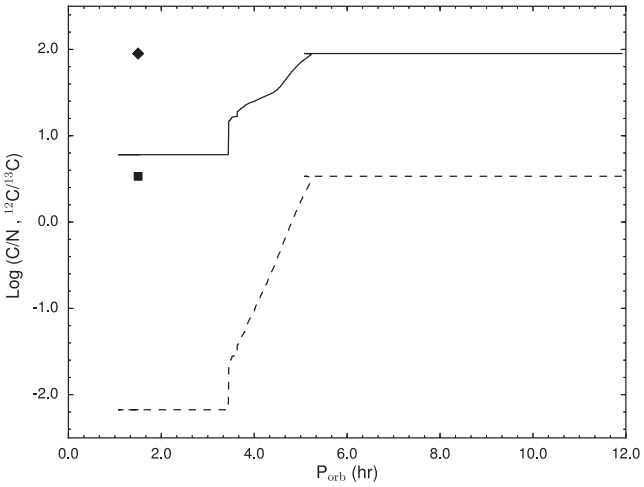

Figure 12. Surface abundance ratios (C/N, dashed line and C_{12}/C_{13}, solid line) for the main-sequence star in TYC 6760-497-1 as a function of orbital period. Once a deep convective envelope forms (P_{orb} ∼5 h), both abundance ratios substantially decrease as carbon-depleted material is dredged up from the inner regions of the star where CNO burning has taken place. In contrast, the abundance ratios of a CV born with a low-mass donor (which never began CNO burning) will remain largely fixed, even when the star becomes fully convective. We show the abundance ratios for such a 'normal' CV (C/N, black square, C_{12}/C_{13}, black diamond).

ratios found by Gänsicke et al. (2003) which are frequently called *failed* SN Ia.

A final note concerning the future of TYC 6760-497-1 concerns the expected white dwarf mass when the systems becomes a CV. The mean white dwarf mass in CVs derived from observations (∼0.8 $M_\odot$; Zorotovic, Schreiber & Gänsicke 2011) is significantly higher than predicted by binary population models of CVs and significantly larger than the mean value observed in CV progenitors containing low-mass secondaries (see Zorotovic et al. 2011, for details). The value predicted by our simulations for TYC 6760-497-1, however, is very close to the mean white dwarf mass of the observed CV sample. One could therefore speculate that if the number of CVs descending from PCEBs with massive secondaries has been underestimated previously, the problem with the white dwarf masses in CVs could be solved. Assuming that a large number of CVs are descendants from PCEBS with massive secondary stars such as TYC 6760-497-1 indeed predicts an increased number of CVs with white dwarf masses ∼0.8 $M_\odot$. However, the large number of CVs with evolved secondaries predicted in this scenario violates the general explanation for the orbital period gap (see Wijnen, Zorotovic & Schreiber 2015, for more details). We therefore believe that the fraction of CVs descending from systems with initially massive secondaries does not significantly exceed the ∼10 per cent of CVs with decreased C/N line ratios as measured by Gänsicke et al. (2003) and the white dwarf mass problem remains to be solved.

We emphasize that the above evolutionary scenario for TYC 6760-497-1 is based on several assumptions such as the strength of magnetic braking, the angular momentum taken away from the system during nova eruptions and the fraction of mass that is lost during thermal time-scale mass transfer. However, our simulation shows that it is likely that TYC 6760-497-1 is the first known progenitor of an SSS.

6 CONCLUSIONS

We have identified TYC 6760-497-1 as a close binary consisting of a white dwarf and an F8 star that is extremely close to filling its Roche lobe. Assuming that the F star is tidally locked, we constrain the masses of the two stars to $M_{WD} = 0.52$–$0.67\,M_\odot$, $M_{MS} = 1.22$–$1.25\,M_\odot$ and the radius of the F star to $R_{MS} = 1.18$–$1.40\,R_\odot$. The white dwarf is still hot (19 500–21 000 K) and so the system only emerged from the common envelope 0.1 Gyr ago. Its progenitor was likely on the TP-AGB when the common envelope began. However, this means that the common envelope efficiency was quite low, in contrast to other systems containing white dwarfs with early-type companions, implying that the efficiency depends upon more than just the mass of the companion star.

TYC 6760-497-1 will become a semi-detached system in less than 5 Myr and will undergo a short phase (∼1 Myr) of thermal time-scale mass transfer in 13.1 Myr resulting in a roughly 20 per cent increase in the white dwarf's mass, still well short of the Chandrasekhar limit, after which it will become a standard CV system.

Although we have placed some constraints on the binary parameters, these will be greatly improved with an accurate distance measurement from *Gaia* which should reach a precision of ∼0.3 per cent at the expected distance of TYC 6760-497-1.[1] This will dramatically reduce the reliance on evolutionary models in our measurements allowing us to more rigorously test the evolutionary scenarios of this (and similar) systems.

ACKNOWLEDGEMENTS

We thank the referee for useful comments and suggestions. SGP, MZ and CT acknowledge financial support from FONDECYT in the form of grant numbers 3140585, 3130559 and 1120338. AB acknowledges financial support from Proyecto FONDECYT de Iniciación 11140572. The research leading to these results has received funding from the European Research Council under the European Union's Seventh Framework Programme (FP/2007-2013)/ERC Grant Agreement no. 320964 (WDTracer). MRS acknowledges support from FONDECYT (1141269) and Millennium Science Initiative, Chilean ministry of Economy: Nucleus RC130007. ARM acknowledges financial support from the Postdoctoral Science Foundation of China (grants 2013M530470 and 2014T70010) and from the Research Fund for International Young Scientists by the National Natural Science Foundation of China (grant 11350110496). RB is supported by CONICYT-PCHA/Doctorado Nacional. RB acknowledges additional support from project IC120009 'Millenium Institute of Astrophysics (MAS)' of the Millennium Science Initiative, Chilean Ministry of Economy. AJ acknowledges support from the Ministry for the Economy, Development, and Tourism's Programa Iniciativa Científica Milenio through grant IC 120009, awarded to the Millennium Institute of Astrophysics (MAS), FONDECYT project 1130857 and from BASAL CATA PFB-06. This work is based on observations made with the NASA/ESA *Hubble Space Telescope*, obtained at the Space Telescope Science Institute, which is operated by the Association of Universities for Research in Astronomy, Inc., under NASA contract NAS 5-26555. These observations are associated with programme #13704. The results presented in this paper are based on observations collected at the European Southern Observatory under

[1] http://www.cosmos.esa.int/web/gaia/science-performance

programme ID 094.D-0344. The FEROS observations were obtained via Max Planck Institute for Astronomy (MPIA) guaranteed time. This publication makes use of VOSA, developed under the Spanish Virtual Observatory project supported from the Spanish MICINN through grant AyA2008-02156.

REFERENCES

Allard F., Homeier D., Freytag B., 2012, Phil. Trans. R. Soc. A, 370, 2765
Bayo A., Rodrigo C., Barrado Y., Navascués D., Solano E., Gutiérrez R., Morales-Calderón M., Allard F., 2008, A&A, 492, 277
Branch D., Tammann G. A., 1992, ARA&A, 30, 359
Bressan A., Marigo P., Girardi L., Salasnich B., Dal Cero C., Rubele S., Nanni A., 2012, MNRAS, 427, 127
Burleigh M. R., Barstow M. A., Fleming T. A., 1997, MNRAS, 287, 381
Camacho J., Torres S., García-Berro E., Zorotovic M., Schreiber M. R., Rebassa-Mansergas A., Nebot Gómez-Morán A., Gänsicke B. T., 2014, A&A, 566, A86
Claret A., 2004, A&A, 428, 1001
Coelho P., Barbuy B., Meléndez J., Schiavon R. P., Castilho B. V., 2005, A&A, 443, 735
D'Odorico S. et al., 2006, Proc. SPIE, 6269, 626933
de Kool M., 1992, A&A, 261, 188
Fink M., Hillebrandt W., Röpke F. K., 2007, A&A, 476, 1133
Fink M., Röpke F. K., Hillebrandt W., Seitenzahl I. R., Sim S. A., Kromer M., 2010, A&A, 514, A53
Fontaine G., Brassard P., Bergeron P., 2001, PASP, 113, 409
Gänsicke B. T. et al., 2003, ApJ, 594, 443
Ge H., Webbink R. F., Chen X., Han Z., 2013, in Zhang C. M., Belloni T., Méndez M., Zhang S. N., eds, Proc. IAU Symp. 290, Feeding Compact Objects: Accretion on All Scales. Cambridge Univ. Press, Cambridge, p. 213
Greiner J., 2000, New Astron., 5, 137
Hjellming M. S., 1989, PhD thesis, Illinois Univ. at Urbana-Champaign, Savoy
Holberg J. B., Oswalt T. D., Sion E. M., Barstow M. A., Burleigh M. R., 2013, MNRAS, 435, 2077
Hubeny I., Lanz T., 1995, ApJ, 439, 875
Hurley J. R., Tout C. A., Pols O. R., 2002, MNRAS, 329, 897
Husser T.-O., Wende-von Berg S., Dreizler S., Homeier D., Reiners A., Barman T., Hauschildt P. H., 2013, A&A, 553, A6
Jordán A. et al., 2014, AJ, 148, 29
Kordopatis G. et al., 2013, AJ, 146, 134
Kruse E., Agol E., 2014, Science, 344, 275
Marsh T. R., 1989, PASP, 101, 1032
Martin D. C. et al., 2005, ApJ, 619, L1
Maxted P. F. L., Gänsicke B. T., Burleigh M. R., Southworth J., Marsh T. R., Napiwotzki R., Nelemans G., Wood P. L., 2009, MNRAS, 400, 2012
Napiwotzki R. et al., 2003, The Messenger, 112, 25
Paczynski B., 1976, in Eggleton P., Mitton S., Whelan J., eds, Proc. IAU Symp. 73, Structure and Evolution of Close Binary Systems. Reidel, Dordrecht, p. 75
Parsons S. G. et al., 2012, MNRAS, 420, 3281
Paxton B., Bildsten L., Dotter A., Herwig F., Lesaffre P., Timmes F., 2011, ApJS, 192, 3
Perlmutter S. et al., 1999, ApJ, 517, 565
Pyrzas S. et al., 2012, MNRAS, 419, 817
Rappaport S., Verbunt F., Joss P. C., 1983, ApJ, 275, 713
Rebassa-Mansergas A., Nebot Gómez-Morán A., Schreiber M. R., Gänsicke B. T., Schwope A., Gallardo J., Koester D., 2012a, MNRAS, 419, 806
Rebassa-Mansergas A. et al., 2012b, MNRAS, 423, 320
Ribeiro T., Baptista R., Kafka S., Dufour P., Gianninas A., Fontaine G., 2013, A&A, 556, A34
Riess A. G. et al., 1998, AJ, 116, 1009
Ritter H., 1988, A&A, 202, 93
Schenker K., Kolb U., Ritter H., 1998, MNRAS, 297, 633
Schenker K., King A. R., Kolb U., Wynn G. A., Zhang Z., 2002, MNRAS, 337, 1105
Schlafly E. F., Finkbeiner D. P., 2011, ApJ, 737, 103
Shen K. J., Moore K., 2014, ApJ, 797, 46
Skrutskie M. F. et al., 2006, AJ, 131, 1163
Tappert C., Gänsicke B. T., Schmidtobreick L., Ribeiro T., 2011, A&A, 532, A129
Toonen S., Nelemans G., 2013, A&A, 557, A87
Torres G., Andersen J., Giménez A., 2010, A&AR, 18, 67
Tout C. A., Pols O. R., Eggleton P. P., Han Z., 1996, MNRAS, 281, 257
Tutukov A., Yungelson L., 1996, MNRAS, 280, 1035
Webbink R. F., 1984, ApJ, 277, 355
Whelan J., Iben I., Jr, 1973, ApJ, 186, 1007
Wijnen T. P. G., Zorotovic M., Schreiber M. R., 2015, A&A, 577, A143
Wonnacott D., Kellett B. J., Stickland D. J., 1993, MNRAS, 262, 277
Wright E. L. et al., 2010, AJ, 140, 1868
Zahn J.-P., 1977, A&A, 57, 383
Zorotovic M., Schreiber M. R., Gänsicke B. T., Nebot Gómez-Morán A., 2010, A&A, 520, A86
Zorotovic M., Schreiber M. R., Gänsicke B. T., 2011, A&A, 536, A42
Zorotovic M., Schreiber M. R., Parsons S. G., 2014, A&A, 568, L9

This paper has been typeset from a TEX/LATEX file prepared by the author.